equatorial plane of the complex (plane A). Free rotation of the η^1-naph ligand will result in the α-proton of that ligand spending a great deal of time in the shielding area above the chelate ligand, and so experiencing an upfield shift.

Warming the phen complex from 273 to 348 K caused a series of NMR changes illustrated in Figure 2. This results in a high-temperature-limit spectrum in which only a simple AMX pattern is distinguishible for the naph ligand, indicating that the α, β, γ and α', β', γ' nuclei are being rendered equivalent by a rapid metal exchange between the two nitrogen atoms in what can be called a 1,3-haptotropic shift.

From the coalescence of the α, α' and β, β' resonances of complex **1** and that of the α, α' resonances of complex **2** an approximate[26] energy barrier of 63 kJ/mol is obtained for the 1,3-haptotropic shift observed in both complexes. Although approximate, this value confirms our previous prediction[16] that, for octahedral complexes of first-row transition metals with an η^1-naph ligand, ΔG^* values for the intramolecular 1,3-haptotropic shift increase in the order Cr(0) {[Cr(η^1-naph)(CO)$_5$], 58.7 kJ/mol}[14] > Mn(I) {[Mn(η^1-naph)(η^2-chel)(CO)$_3$]$^+$ (chel = phen, bpy), 63 kJ/mol)} > Fe(II) {[Fe(η^1-naph)(CO)$_2$Cp]$^+$, $\gg$71 kJ/mol}.[15]

Mechanism of the Fluxional Process. In order to obtain information on the fluxional process, two different experiments were undertaken. First, the ^{1}H NMR spectra of acetone-d_6 solutions of complexes **1** and **2** at the coalescence temperature were obtained and no changes were observed when the samples were diluted first to half and then to one-fourth of the initial concentration. In the second experiment free naph was added to solutions of complexes **1** and **2** and their ^{1}H NMR spectra at 308 K were obtained: For both complexes the overlap between the α and β resonances of the free and coordinated 1,8-naphthyridine was very extensive, but the low-field doublet of the γ-proton of the coordinated naph ligand was clearly observed and not affected by the presence of free amine. These experiments showed that the 1,3-haptotropic shift was unimolecular, the only species involved being the complex itself. Thus, the mechanism for the fluxional exchange could either be intramolecular, involving a seven-coordinated manganese, or proceed through a 16-electron [MnL$_5$]$^+$/noninteracting 1,8-naphthyridine intermediate caught in the solvent cage. Our experimental results cannot distinguish between these two possible mechanisms. EH-MO calculations of the metal 1,3-haptotropic shift in the complex [Cr(η^1-naph)(CO)$_5$] have shown that the transition state contains substantial dissociative character, but due to the favorable orientation of the nitrogen lone pairs of the naphthyridine, some bonding interaction is still left.[27] According to that, we can speculate that for the naphthyridine complexes of manganese(I) reported in this paper the transition state for the 1,3-shift cannot be explained in terms of either a seven- or a five-coordinated manganese species but in terms of a concerted mechanism in which bond breaking is fundamental but some degree of interaction between the metal and the naphthyridine is kept throughout the reaction path.

Registry No. **1**, 116634-49-2; **2**, 116634-51-6; [MnBr(phen)(CO)$_3$], 56811-95-1; [MnBr(bpy)(CO)$_3$], 38173-71-6.

Supplementary Material Available: Tables of the crystal data collection and refinement, anisotropic thermal parameters and final hydrogen atom coordinates, all bond lengths and angles (hydrogen and non-hydrogen atoms), and the most important least-squares planes and deviations therefrom (10 pages); a listing of observed and calculated structure factors (9 pages). Ordering information is given on any current masthead page.

(26) Derived from the equation $\Delta G^* = 2.303RT_c(10.319 - \log k' + \log T_c)$, where T_c is the coalescence temperature and $k' = \pi(\Delta\nu)/2^{1/2}$: Calder, I. C.; Garrat, P. J. *J. Chem. Soc. B* **1967**, 660. $\Delta\nu$ is the frequency separation of the coalescing peaks, and the equation is strictly valid only for coalescence of two singlets. Consequently, the present results should be used only as an approximate indication of ΔG^*.

(27) Kang, S.-K.; Albright, T. A.; Mealli, C. *Inorg. Chem.* **1987**, *26*, 3158.

Contribution from the Department of Chemistry,
University of Houston—University Park, Houston, Texas 77204-5641

Dipalladium Complexes with *N,N'*-Diphenylbenzamidine Bridging and Chelating Ligands. Synthesis and Structural and Electrochemical Studies

C.-L. Yao, L.-P. He, J. D. Korp, and J. L. Bear*

Received May 12, 1988

The reaction of the palladium acetate trimer, Pd$_3$(OOCCH$_3$)$_6$, with lithium *N,N'*-diphenylbenzamidinate, Li(dpb), in CH_2Cl_2 gives a product with molecular formula Pd$_2$(dpb)$_4$. A single-crystal X-ray structure analysis shows the complex to contain two palladium(II) ions bridged by two dpb ligands, with an additional dpb ion chelated to each of the metals forming four-membered rings, [(dpb)Pd]$_2$(μ-dpb)$_2$ (**1**). Compound **1**, $C_{76}H_{60}N_8Pd_2\cdot H_2O\cdot CH_3OH$, crystallizes as large reddish orange parallelepipeds in space group $C2/c$ with 8 formula weights in a unit cell of dimensions a = 32.319 (7) Å, b = 22.396 (5) Å, c = 24.970 (5) Å, and β = 121.29 (1)°. Since there is no formal Pd···Pd bond, interligand repulsion of the bulky dpb molecules forces apart the the chelating groups, resulting in a dihedral angle between the two Pd(N)$_4$ coordination planes of 35° and a Pd···Pd separation of 2.90 Å. When **1** is refluxed in methanol, the two chelating ligands rearrange to form the tetrabridged complex, Pd$_2$(μ-dpb)$_4$ (**2**). Compound **2**, $C_{76}H_{60}N_8Pd_2\cdot C_2H_6O$, crystallizes as bright red columns in the orthorhombic space group *Pbca* with 8 formula weights in a unit cell of dimensions a = 22.230 (7) Å, b = 24.483 (9) Å, and c = 24.140 (9) Å. The Pd···Pd separation is 2.58 Å, and the two Pd(N)$_4$ coordination planes have an average torsion angle of 14.1°. The oxidation potentials of **1** and **2** show an effect on the HOMO's of the two molecules due to the proximity of the two palladium ions. Both of the two noninteracting palladium ions of **1** are oxidized irreversibly at 1.02 V vs SCE in CH_2Cl_2, 0.1 M TBAP, whereas under the same conditions **2** undergoes a reversible one-electron oxidation at 0.65 V to form the cation-radical complex [Pd^{II}Pd^{III}(μ-dpb)$_4$]$^+$. No other reversible cyclic wave was observed up to the potential limit of the solvent. The ESR spectrum of [Pd^{II}Pd^{III}(μ-dpb)$_4$]$^+$ clearly shows an axial signal with $g_\perp$ = 2.17 and $g_\parallel$ = 1.98. Satellite peaks due to ^{105}Pd ($I = {}^5/_2$, natural abundance 22.3%) are observed. The ESR spectrum is similar to that of the isoelectronic [Rh^{I}Rh^{II}(μ-dpb)$_4$]$^-$ complex and shows that the oxidation is metal centered.

Introduction

Among the dinuclear transition-metal complexes, the dirhodium compounds are the most sensitive to the nature of the axial and bridging ligands with respect to variation in their chemical and electrochemical behavior. This sensitivity is due, in a large part, to the high occupancy of the M–M antibonding molecular orbitals. Dirhodium(II) complexes with strong electron-pair-donor bridging ligands can be readily oxidized by two successive and reversible one-electron processes to produce the Rh^{II}Rh^{III} and Rh$^{III}_2$ oxidation states.[1-5] However, there are few examples of Rh$^{II}_2$ complexes

(1) Duncan, J.; Malinski, T.; Zhu, T. P.; Hu, Z. S.; Kadish, K. M.; Bear, J. L. *J. Am. Chem. Soc.* **1982**, *104*, 5507.
(2) Chavan, M. Y.; Zhu, T. P.; Lin, X. Q.; Ahsan, M. Q.; Bear, J. L.; Kadish, K. M. *Inorg. Chem.* **1984**, *23*, 4538.

0020-1669/88/1327-4389$01.50/0

which contain anionic bridging ligands that undergo a metal-centered reversible reduction to form the $Rh^{I}Rh^{II}$ oxidation state. The complexes that have been reported are the tetrabridged *N,N'*-diphenylbenzamidinate (dpb), *N,N'*-diphenylformamidinate (dpf), and *N,N'*-di-*p*-tolylformamidinate (dtf) compounds. In all cases the $Rh^{I}Rh^{II}$ product is highly reactive and unstable.[3,6] However, the complex $Rh^{I}Rh^{II}(dpb)_4$ is sufficiently stable to measure its ESR spectrum whereas $Rh^{I}Rh^{II}(dpf)_4$ is not.

Dipalladium(II) complexes with bridging ligands that force axial symmetry and stabilize higher oxidation states could lead to the formation of stable $Pd^{II}Pd^{III}$ and Pd^{III}_2 compounds. Complexes of the latter oxidation state would be isoelectronic with Rh^{II}_2 compounds, and those of $Pd^{II}Pd^{III}$ would have a bond order of 0.5 and be isoelectronic with $Rh^{I}Rh^{II}$ compounds. Therefore, dipalladium(II), -(II,III), and -(III) complexes offer the opportunity to investigate weak M–M interactions beyond that of the dirhodium system and to evaluate the sensitivity of the metal-centered molecular orbitals of the dipalladium cation to inductive effects and polarization by equatorial and axial ligands.

The syntheses and molecular structures of several dipalladium(II) complexes have been reported in recent years. They include the bridging ions 2-hydroxypyridinate,[7,8] dithioacetate,[9] 1,3-benzothiazole-2-thiolate,[10] and *N,N'*-di-*p*-tolylformamidinate.[11] It is also interesting that in the attempt to study the tolylbenzothiazole and tolylbenzoxazole substitution reactions with $Pd_3(O\text{-}OCCH_3)_6$, Churchill et al. successfully isolated and characterized complexes that have two acetate bridging ligands and two tolylbenzothiazole or tolylbenzoxazole molecules functioning as five-membered-ring chelating ligands.[12] Electrochemical study showed that $Pd^{II}_2(\mu\text{-dtf})_4$ underwent two reversible one-electron oxidations with $E_{1/2} = +0.81$ and $+1.19$ V vs Ag/AgCl in CH_2Cl_2, 0.1 M in $(TBA)PF_6$.[11] The cyclic waves were assigned to the formation of $[Pd^{II}Pd^{III}(\mu\text{-dtf})_4]^+$ and $[Pd^{III}_2(\mu\text{-dtf})_4]^{2+}$. Attempts to isolate the higher oxidation state complexes were not successful. The ESR spectrum of the mixed-valence complex, $[Pd^{II}Pd^{III}(\mu\text{-dtf})_4]^+$, shows only a single symmetric signal at liquid-nitrogen temperature.[11] This is a surprising result since the molecule possesses axial symmetry and is isoelectronic with $[Rh^{I}Rh^{II}(\mu\text{-dpb})_4]^-$, which gives an axial ESR signal.[3]

In this paper, we present the syntheses, X-ray crystal structures, and electrochemical properties of *cis*-bis(μ-*N,N'*-diphenylbenzamidinato)bis(*N,N'*-diphenylbenazmidinato)dipalladium(II), $[(dpb)Pd]_2(\mu\text{-dpb})_2$ (**1**), and tetrakis(μ-*N,N'*-diphenylbenzamidinato)dipalladium(II), $Pd^{II}_2(\mu\text{-dpb})_4$ (**2**). Compound **1** is a reaction intermediate, which has two dpb bridging ligands and two dpb chelating ligands, formed in the reaction of palladium acetate with Li(dpb). The electrochemistry of both complexes was carried out in CH_2Cl_2, and the redox potentials and ESR spectra are reported. The results are quite different from those reported for $Pd_2(\mu\text{-dtf})_4$.[11] In addition, the effect of the proximity of the two palladium ions in **1** and **2** on the thermodynamics of the electron-transfer reaction is evaluated.

Experimental Section

Synthesis of $[(dpb)Pd]_2(\mu\text{-dpb})_2$. Compound **1** was synthesized by the reaction of 0.30 g of palladium acetate (0.444 mmol) with 0.74 g of Li(dpb) (2.664 mmol) in CH_2Cl_2 at room temperature for 14 h. The solvent was removed from the reaction mixture by using a rotary evaporator. The solid was dissolved in a minimum amount of CH_2Cl_2 first and then the solution added slowly to 250 mL of CH_3OH. The solution was stirred overnight at room temperature. The orange precipitate was then removed by filtration. The solid was dissolved in CH_2Cl_2 and purified on a silica gel column three times with 1/20 CH_3OH/CH_2Cl_2 as the eluent. The reddish orange band was collected as the pure product. Due to the extensive purification procedure, the yield was only 14%, based on the amount of the starting palladium acetate. Crystals suitable for X-ray diffraction were grown by slow evaporation of a CH_2Cl_2/CH_3OH/hexane solution. The UV–visible spectrum of the complex shows two absorption peaks on the edge of a strong band extending into the UV region at 378 ($\epsilon = 2.4 \times 10^4$) and 496 nm ($\epsilon = 3.6 \times 10^3$).

Synthesis of $Pd_2(\mu\text{-dpb})_4$. Compound **2** was prepared by refluxing a 50-mL CH_3OH solution containing 50 mg of $[(dpb)Pd]_2(\mu\text{-dpb})_2$ for 2 h. The color of the complex turned from orange to reddish, and some demetalation was also observed in the form of a light Pd mirror on the glassware. Prolonged heating was avoided to prevent further demetalation. The solvent was removed and the solid recrystallized from a CH_2Cl_2/C_2H_5OH solution. At this stage the solid was a mixture of two palladium complexes, which were separated on an alumina column using a 1/1 mixture of CH_2Cl_2 and hexane. The first band, which corresponded to compound **2**, was collected, and the yield of **2** was 40%. The second band was due to a minor product that we have been unable to structurally characterize at the present time. Compound **2** shows a broad absorbance in the visible region centered at 500 nm, ($\epsilon = 2.5 \times 10^3$) and a much stronger absorbance in the UV region with multiple shoulders extending into the visible region.

Reagents and Instrumentation. All solvents were purified by standard literature methods.[13] Tetrabutylammonium perchlorate (TBAP) was twice recrystallized from ethanol. Cyclic voltammetric measurements were made by using the conventional three-electrode configuration and recorded on an IBM Model EC225 voltammetric analyzer. The working electrode was a platinum button with a calibrated area of 0.19 mm^2, and a saturated calomel electrode (SCE) was used as reference. ESR measurements were carried out on a Bruker Model 100D spectrometer.

X-ray Crystallography

$[(dpb)Pd]_2(\mu\text{-dpb})_2$. A large reddish orange parallelepiped having approximate dimensions 0.55 × 0.40 × 0.15 mm was mounted in a random orientation on a Nicolet R3m/V automatic diffractometer. The crystal had to be mounted inside a thin-walled glass capillary tube filled with mother liquor (a mixture of hexane, methanol, methylene chloride, and trace water), since the crystal sample showed almost instantaneous decomposition upon removal from solvents. The radiation used was Mo Kα monochromatized by a highly ordered graphite crystal. Final cell constants, as well as other information pertinent to data collection and refinement, are listed in Table I. The Laue symmetry was determined to be $2/m$, and the space group was shown to be either $C2/c$ or Cc. Intensities were measured by using the ω-scan technique, with the scan rate depending on the count obtained in rapid prescans of each reflection. Two standard reflections were monitored after every 2 h or every 100 data collected, and these showed no significant variation. In the reduction of the data, Lorentz and polarization corrections were applied; however, no correction for absorption was made due to the small absorption coefficient.

The structure was solved by use of the SHELXTL Patterson interpretation program, which revealed the positions of the two Pd atoms in the

Table I. Data Collection and Processing Parameters

	$[(dpb)Pd]_2(\mu\text{-dpb})_2$ (**1**)	$Pd_2(\mu\text{-dpb})_4$ (**2**)
space group	$C2/c$	$Pbca$
cell constants		
a, Å	32.319 (7)	22.230 (7)
b, Å	22.396 (5)	24.483 (9)
c, Å	24.970 (5)	24.140 (9)
β, deg	121.29 (1)	
V, Å^3	15444	13138
molecular formula	$C_{76}H_{60}N_8Pd_2\cdot H_2O\cdot CH_3OH$	$C_{76}H_{60}N_8Pd_2\cdot C_2H_6O$
fw	1348.3	1298.2
Z	8	8
ρ(calc), g cm^{-3}	1.16	1.31
μ, cm^{-1}	5.02	5.86
λ(Mo Kα), Å	0.71073	0.71073
$R(F_o)$	0.059	0.049
$R_w(F_o)$	0.069	0.041

(3) Le, J. C.; Chavan, M. Y.; Chau, L. K.; Bear, J. L.; Kadish, K. M. *J. Am. Chem. Soc.* **1985**, *107*, 7195.
(4) Lifsey, R. S.; Chavan, M. Y.; Chau, L. K.; Ahsan, M. Q.; Kadish, K. M.; Bear, J. L. *Inorg. Chem.* **1987**, *26*, 822.
(5) Bear, J. L.; Liu, L-M.; Kadish, K. M. *Inorg. Chem.* **1987**, *26*, 2927.
(6) Lifsey, R. S. Ph.D. Dissertation, University of Houston, 1987.
(7) Clegg, W.; Garner, C. D.; Al-Samman, M. H. *Inorg. Chem.* **1982**, *21*, 1897.
(8) Bancroft, P.; Cotton, F. A.; Falvello, L. R.; Schwotzer, W. *Inorg. Chem.* **1986**, *25*, 1015.
(9) Piovesana, O.; Bellitto, C.; Flamini, A.; Zanazzi, P. F. *Inorg. Chem.* **1979**, *18*, 2258.
(10) Kubiak, M. *Acta Crystallogr.* **1985**, *C41*, 1288.
(11) Cotton, F. A.; Matusz, M.; Poli, R. *Inorg. Chem.* **1987**, *26*, 1472.
(12) Churchill, M. R.; Wasserman, H. J.; Young, G. J. *Inorg. Chem.* **1980**, *19*, 762.
(13) Perrin, D. D.; Armrego, W. L. F.; Perrin, D. R. *Purification of Laboratory Chemicals*; Pergamon: New York, 1980.

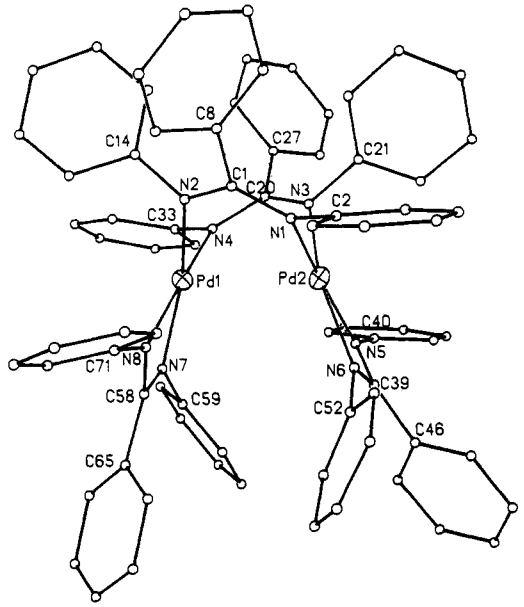

Figure 1. Labeling of key atoms in $[(dpb)Pd]_2(\mu\text{-dpb})_2$ (**1**).

asymmetric unit, comprising one complete molecule. The remaining non-hydrogen atoms were located in subsequent difference Fourier syntheses. Due to the very large number of atoms involved, only the Pd and N atoms were refined anisotropically. Hydrogens were added in ideal calculated positions with a single nonvariable isotropic thermal parameter for all of them. At this point, an area of heavily disordered solvent was found and determined to be composed of several separate molecules. Two of these (O(77) and O(78)) showed no close contacts whatsoever and thus are assumed to be water molecules. Reasonable isotropic thermal parameters for these atoms were obtained by fixing the population factors at 60% and 40%, respectively. The remaining residual density was best accounted for by assuming it to be due to four pairs of atoms, presumably from methanols, each having an occupancy factor of approximately 25%. All solvent atoms were allowed to refine independently, although no attempt was made to include hydrogens due to the extremely low occupancies. After all shift/esd ratios were less than 0.4 (except for the solvent atoms), convergence was reached at the agreement factors listed in Table I. No unusually high correlations were noted between any of the variables in the last cycle of full-matrix least-squares refinement, and the final difference density map showed no peak greater than 0.5 e/Å^3.

$Pd_2(\mu\text{-dpb})_4$. A small, bright red square column having approximate dimensions 0.12 × 0.12 × 0.50 mm was mounted in a random orientation on the diffractometer. The sample was initially uniformly translucent, but during the 2 h of preliminary measurements it was noted to develop extensive cracks. Final cell constants, as well as other information pertinent to data collection and refinement, are listed in Table I. The Laue symmetry was determined to be *mmm*, and the space group was shown unambiguously to be *Pbca*.

The structure solution and refinement procedures were the same as above. A molecule of solvation was found, presumably ethanol, which is initially present in full occupancy at this site but quickly evacuates upon exposure to X-rays, leading to the observed crystal cracking mentioned above. After all shift/esd ratios were less than 0.2 (except for the solvent atoms), convergence was reached at the agreement factors listed in Table I. The final difference density map showed no peak greater than 0.4 e/Å^3.

Results and Discussion

Structure of $[(dpb)Pd]_2(\mu\text{-dpb})_2$. A structural view of the dinuclear unit is shown in Figure 1. Tables II and III list some selected bond lengths and angles. Table IV contains the final positional and thermal parameters for the complex. Figure 1 shows two dpb bridging ligands cis to each other, with the remaining two dpb ions acting as bidentate chelating ligands, which form four-membered rings with separate palladium atoms. Since there is no formal metal–metal bond in this Pd(II)–Pd(II) complex, the interligand repulsion of the bulky dpb molecules easily forces apart the chelating groups, resulting in the Pd–Pd separation of 2.90 Å. This value is somewhat larger than those noted in similar benzoxazole and benzothiazole complexes having acetate bridges[12] and somewhat smaller than those found in more exotic systems.[14,15]

Table II. Selected Bond Lengths (Å)

	$[(dpb)Pd]_2(\mu\text{-dpb})_2$ (**1**)		
Pd(1)–N(2)	2.03 (1)	Pd(1)–N(4)	2.04 (1)
Pd(1)–N(7)	2.09 (1)	Pd(1)–N(8)	2.00 (1)
Pd(2)–N(1)	2.05 (1)	Pd(2)–N(3)	2.01 (1)
Pd(2)–N(5)	2.03 (1)	Pd(2)–N(6)	2.10 (2)
N(1)–C(1)	1.33 (2)	N(1)–C(2)	1.43 (2)
N(2)–C(1)	1.33 (2)	N(2)–C(14)	1.39 (2)
N(3)–C(20)	1.30 (2)	N(3)–C(21)	1.42 (2)
N(4)–C(20)	1.34 (2)	N(4)–C(33)	1.40 (2)
N(5)–C(39)	1.32 (2)	N(5)–C(40)	1.39 (2)
N(6)–C(39)	1.35 (2)	N(6)–C(52)	1.37 (2)
N(7)–C(58)	1.31 (2)	N(7)–C(59)	1.42 (2)
N(8)–C(58)	1.34 (2)	N(8)–C(71)	1.38 (2)
C(1)–C(8)	1.54 (2)	C(20)–C(27)	1.51 (2)
C(39)–C(46)	1.51 (2)	C(58)–C(65)	1.51 (2)
O(80)–C(81)	1.27 (7)	O(82)–C(83)	1.48 (9)
O(84)–C(85)	1.33 (7)	O(86)–C(87)	1.80 (9)
Pd(1)···Pd(2)	2.900 (1)		
	$Pd_2(\mu\text{-dpb})_4$ (**2**)		
Pd(1)–N(1)	2.05 (1)	Pd(1)–N(3)	2.05 (1)
Pd(1)–N(5)	2.05 (1)	Pd(1)–N(7)	2.05 (1)
Pd(2)–N(2)	2.07 (1)	Pd(2)–N(4)	2.03 (1)
Pd(2)–N(6)	2.06 (1)	Pd(2)–N(8)	2.04 (1)
N(1)–C(1)	1.31 (1)	N(1)–C(2)	1.42 (1)
N(2)–C(1)	1.32 (1)	N(2)–C(14)	1.44 (1)
N(3)–C(20)	1.33 (1)	N(3)–C(21)	1.43 (1)
N(4)–C(20)	1.33 (1)	N(4)–C(33)	1.43 (1)
N(5)–C(39)	1.33 (1)	N(5)–C(40)	1.41 (1)
N(6)–C(39)	1.30 (1)	N(6)–C(52)	1.42 (1)
N(7)–C(58)	1.30 (1)	N(7)–C(59)	1.42 (1)
N(8)–C(58)	1.34 (1)	N(8)–C(71)	1.41 (1)
C(1)–C(8)	1.50 (1)	C(20)–C(27)	1.49 (1)
C(39)–C(46)	1.53 (1)	C(58)–C(65)	1.52 (1)
O–C(78)	1.52 (7)	C(77)–C(78)	1.49 (8)
Pd(1)···Pd(2)	2.576 (1)		

The dihedral angle between the two $Pd(N)_4$ coordination planes is 35°, which is considerably greater than the 24° angle found in the benzoxazole and benzothiazole complexes,[12] indicating much greater steric repulsion in the present case. For reference, the interatomic spacing in palladium metal is 2.75 Å.[16] In addition, the average C–N–Pd angle here is 124° vs the expected 120° for an sp^2 nitrogen. Some further relief of the strain is found in the larger than usual 19° N–Pd···Pd–N torsion angle, which tends to stagger the chelating ligands.

Despite the radically different geometric constraints placed on the bridging and chelating ligands, the observed average Pd–N, N–C(amidine), and N–C(phenyl) bond distances show essentially no differences. The bond angles, however, are by necessity substantially less obtuse in the chelating ligand (C–N–Pd = 93°). The formation of a four-membered ring results in a 64° angle at Pd; however, angles as small as 60° have been found in other stable metal complexes such as Rh(1,3-diphenyltriazine)$_3$.[17] There is probably some strain in this small angle, and this could be a factor in the enhanced reactivity of the complex toward rearrangement to the tetrabridged compound. When five-member rings are formed in complexes with similar structures, such as $[(tolylbenzothiazole)Pd]_2(\mu\text{-}OOCCH_3)_2$ or $[(tolylbenzoxazole)Pd]_2(\mu\text{-}OOCCH_3)_2$, the N–Pd–C bond angles are 81.17 and 80.39°,[12] respectively, and rearrangement is not observed. The dinuclear unit has approximate C_2 symmetry, but slight disorientation of the phenyl groups violates the overall symmetry.

The configuration of the tetrabridged complex is shown in Figure 2, and selected bonding geometries are given in Tables II and III, based on the atomic coordinates shown in Table IV. The dinuclear unit has essentially D_4 symmetry, neglecting some slight

(14) Zocchi, M.; Tieghi, G.; Albinati, A. *J. Chem. Soc., Dalton Trans.* **1973**, 883.
(15) Wong-Ng, W.; Cheng, P.-T.; Kocman, V.; Luth, H.; Nyburg, S. C. *Inorg. Chem.* **1979**, *18*, 2620.
(16) Donohue, J. *The Structure of Elements*; Wiley: New York, 1976; p 216.
(17) Lifsey, R. S.; Korp, J. D.; Bear, J. L., unpublished results.

Table III. Selected Bond Angles (deg)

			[(dpb)Pd]$_2$(μ-dpb)$_2$ (**1**)				
N(4)-Pd(1)-N(2)	89.9 (5)	N(7)-Pd(1)-N(2)	163.1 (6)	N(2)-C(1)-N(1)	124.7 (16)	C(8)-C(1)-N(1)	117.9 (17)
N(7)-Pd(1)-N(4)	106.0 (6)	N(8)-Pd(1)-N(2)	100.1 (5)	C(8)-C(1)-N(2)	117.4 (17)	C(3)-C(2)-N(1)	118.7 (16)
N(8)-Pd(1)-N(4)	169.7 (6)	N(8)-Pd(1)-N(7)	63.8 (5)	C(7)-C(2)-N(1)	121.7 (17)	C(9)-C(8)-C(1)	120.8 (16)
N(3)-Pd(2)-N(1)	89.8 (5)	N(5)-Pd(2)-N(1)	169.5 (6)	C(13)-C(8)-C(1)	119.1 (15)	C(15)-C(14)-N(2)	122.3 (16)
N(5)-Pd(2)-N(3)	99.2 (6)	N(6)-Pd(2)-N(1)	106.3 (6)	C(19)-C(14)-N(2)	118.2 (15)	N(4)-C(20)-N(3)	121.5 (16)
N(6)-Pd(2)-N(3)	161.3 (6)	N(6)-Pd(2)-N(5)	63.9 (6)	C(27)-C(20)-N(3)	120.3 (18)	C(27)-C(20)-N(4)	118.2 (18)
C(1)-N(1)-Pd(2)	121.5 (11)	C(2)-N(1)-Pd(2)	115.9 (11)	C(22)-C(21)-N(3)	118.7 (17)	C(26)-C(21)-N(3)	123.1 (17)
C(2)-N(1)-C(1)	122.6 (15)	C(1)-N(2)-Pd(1)	124.5 (12)	C(28)-C(27)-C(20)	121.6 (18)	C(32)-C(27)-C(20)	121.0 (17)
C(14)-N(2)-Pd(1)	114.2 (10)	C(14)-N(2)-C(1)	121.3 (14)	C(34)-C(33)-N(4)	122.1 (18)	C(38)-C(33)-N(4)	121.5 (18)
C(20)-N(3)-Pd(2)	127.7 (12)	C(21)-N(3)-Pd(2)	112.3 (11)	N(6)-C(39)-N(5)	110.0 (18)	C(46)-C(39)-N(5)	124.7 (20)
C(21)-N(3)-C(21)	119.9 (15)	C(20)-N(4)-Pd(1)	122.7 (12)	C(46)-C(39)-N(6)	125.2 (20)	C(41)-C(40)-N(5)	122.8 (19)
C(33)-N(4)-Pd(1)	115.2 (12)	C(33)-N(4)-C(20)	122.1 (16)	C(45)-C(40)-N(5)	116.1 (18)	C(47)-C(46)-C(39)	118.7 (18)
C(39)-N(5)-Pd(2)	94.5 (12)	C(40)-N(5)-Pd(2)	134.4 (12)	C(51)-C(46)-C(39)	119.0 (19)	C(53)-C(52)-N(6)	123.0 (19)
C(40)-N(5)-C(39)	127.9 (17)	C(39)-N(6)-Pd(2)	91.0 (12)	C(57)-C(52)-N(6)	120.0 (18)	N(8)-C(58)-N(7)	109.4 (16)
C(52)-N(6)-Pd(2)	143.9 (14)	C(52)-N(6)-C(39)	123.3 (17)	C(65)-C(58)-N(7)	127.2 (18)	C(65)-C(58)-N(8)	123.4 (19)
C(58)-N(7)-Pd(1)	92.0 (12)	C(59)-N(7)-Pd(1)	137.5 (12)	C(60)-C(59)-N(7)	120.8 (18)	C(64)-C(59)-N(7)	118.0 (18)
C(59)-N(7)-C(58)	124.5 (16)	C(58)-N(8)-Pd(1)	94.6 (12)	C(66)-C(65)-C(58)	119.9 (17)	C(70)-C(65)-C(58)	119.9 (18)
C(71)-N(8)-Pd(1)	138.3 (12)	C(71)-N(8)-C(58)	125.7 (17)	C(72)-C(71)-N(8)	116.2 (19)	C(76)-C(71)-N(8)	125.5 (19)
			Pd_2(μ-dpb)$_4$ (**2**)				
N(1)-Pd(1)-Pd(2)	85.9 (3)	N(3)-Pd(1)-Pd(2)	85.2 (3)	C(71)-N(8)-Pd(2)	115.1 (7)	C(71)-N(8)-C(58)	123.7 (11)
N(3)-Pd(1)-N(1)	89.6 (4)	N(5)-Pd(1)-Pd(2)	86.4 (3)	N(2)-C(1)-N(1)	123.4 (12)	C(8)-C(1)-N(1)	118.5 (12)
N(5)-Pd(1)-N(1)	172.3 (4)	N(5)-Pd(1)-N(3)	90.5 (4)	C(8)-C(1)-N(2)	118.1 (12)	C(3)-C(2)-N(1)	119.9 (5)
N(7)-Pd(1)-Pd(2)	85.4 (3)	N(7)-Pd(1)-N(1)	89.9 (4)	C(7)-C(2)-N(1)	119.8 (5)	C(9)-C(8)-C(1)	121.0 (6)
N(7)-Pd(1)-N(3)	170.6 (4)	N(7)-Pd(1)-N(5)	88.7 (4)	C(13)-C(8)-C(1)	119.0 (6)	C(15)-C(14)-N(2)	119.3 (5)
N(2)-Pd(2)-Pd(1)	85.4 (3)	N(4)-Pd(2)-Pd(1)	86.3 (3)	C(19)-C(14)-N(2)	120.5 (5)	N(4)-C(20)-N(3)	122.1 (12)
N(4)-Pd(2)-N(2)	89.8 (4)	N(6)-Pd(2)-Pd(1)	85.3 (3)	C(27)-C(20)-N(3)	120.3 (12)	C(27)-C(20)-N(4)	117.6 (12)
N(6)-Pd(2)-N(2)	170.7 (4)	N(6)-Pd(2)-N(4)	89.1 (4)	C(22)-C(21)-N(3)	121.0 (5)	C(26)-C(21)-N(3)	119.0 (5)
N(8)-Pd(2)-Pd(1)	85.7 (3)	N(8)-Pd(2)-N(2)	89.8 (4)	C(28)-C(27)-C(20)	120.9 (7)	C(32)-C(27)-C(20)	119.1 (7)
N(8)-Pd(2)-N(4)	172.0 (4)	N(8)-Pd(2)-N(6)	89.9 (4)	C(34)-C(33)-N(4)	118.4 (6)	C(38)-C(33)-N(4)	121.3 (6)
C(1)-N(1)-Pd(1)	120.7 (9)	C(2)-N(1)-Pd(1)	116.1 (7)	N(6)-C(39)-N(5)	125.1 (12)	C(46)-C(39)-N(5)	117.8 (12)
C(2)-N(1)-C(1)	122.0 (10)	C(1)-N(2)-Pd(2)	120.5 (9)	C(46)-C(39)-N(6)	117.1 (12)	C(41)-C(40)-N(5)	122.6 (6)
C(14)-N(2)-Pd(2)	116.6 (7)	C(14)-N(2)-C(1)	121.4 (10)	C(45)-C(40)-N(5)	117.3 (6)	C(47)-C(46)-C(39)	119.4 (7)
C(20)-N(3)-Pd(1)	121.3 (8)	C(21)-N(3)-Pd(1)	118.5 (7)	C(51)-C(46)-C(39)	120.5 (7)	C(53)-C(52)-N(6)	119.6 (6)
C(21)-N(3)-C(20)	119.4 (10)	C(20)-N(4)-Pd(2)	121.1 (9)	C(57)-C(52)-N(6)	120.1 (6)	N(8)-C(58)-N(7)	122.6 (12)
C(33)-N(4)-Pd(2)	115.2 (7)	C(33)-N(4)-C(20)	123.0 (10)	C(65)-C(58)-N(7)	119.6 (13)	C(65)-C(58)-N(8)	117.8 (12)
C(39)-N(5)-Pd(1)	119.5 (9)	C(40)-N(5)-Pd(1)	117.4 (7)	C(60)-C(59)-N(7)	120.9 (6)	C(64)-C(59)-N(7)	118.7 (6)
C(40)-N(5)-C(39)	122.3 (11)	C(39)-N(6)-Pd(2)	120.4 (9)	C(66)-C(65)-C(58)	119.7 (7)	C(70)-C(65)-C(58)	120.3 (7)
C(52)-N(6)-Pd(2)	118.1 (7)	C(52)-N(6)-C(39)	121.1 (11)	C(72)-C(71)-N(8)	121.6 (6)	C(76)-C(71)-N(8)	118.4 (6)
C(58)-N(7)-Pd(1)	121.6 (9)	C(59)-N(7)-Pd(1)	117.0 (7)	C(77)-C(78)-O	94 (5)		
C(59)-N(7)-C(58)	120.8 (11)	C(58)-N(8)-Pd(2)	120.7 (8)				

deviations in phenyl ring orientations. The Pd···Pd separation is 2.58 Å, which is slightly shorter than the 2.62 Å observed in Pd_2(μ-dtf)$_4$.[11] The same trend is observed in the corresponding dirhodium complexes, with the Rh–Rh bond in the dpb complex (2.39 Å)[3] somewhat shorter than that in the dtf complex (2.43 Å).[18] The average Pd–N, N–C(amidine), and N–C(phenyl) distances are insignificantly different from those observed in **1**. The mean N–Pd···Pd–N torsion angle is 14°, which is comparable to 15° reported for the dtf analogue.[11]

In both **1** and **2**, the crystals contain excess solvents of crystallization; however, these do not interact with the palladium centers at the axial sites. When **1** and **2** are compared, the most obvious difference is of course the change in metal–metal separation. There are several factors involved, namely the size of the bridging ligand bite, the torsion angle across the metals, the attraction or repulsion of the nonbonded metals, and the steric repulsion of the ligands in the case of the chelating complex. As mentioned above, in **1** as well as other dipalladium compounds having metal separations around 2.9 Å,[12,14,15] there are obvious steric repulsions of the ligands opposite the cis bridges that force the metals to larger than expected distances. On the other hand, if the value of 2.75 Å found in palladium metal is taken as a bench mark, it appears that the tetrabridged complexes having N- or O-bonded ligands tend to draw the metals closer than expected. Some evidence for this may be found by examining the metal separations and the N_4 plane separations. In **2**, the N_4 planes are 2.27 Å apart vs a Pd···Pd separation of 2.58 Å, whereas in the tetrabridged dithioacetate compound, the S_4 planes are 0.14 Å further apart than the two palladiums.[9] The authors concluded

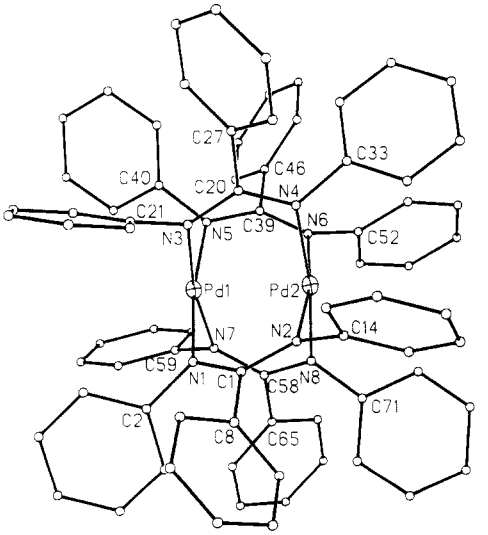

Figure 2. Labeling of key atoms in Pd_2(μ-dpb)$_4$ (**2**).

that there must be a strong Pd···Pd attractive interaction in this case, although the tendency for sp^3-hybridized sulfurs to adopt angles close to 109° may also be an influencing factor in determining the Pd···Pd distance (2.74 Å). When all of the evidence is examined, however, it appears likely that a Pd···Pd separation of 2.75 Å is most energetically favored, and any deviations are caused by external forces inherent to the nature of the ligands.

To the best of our knowledge, no other pair of intermediate chelating and final tetrabridging products has been reported in the literature with X-ray structure analyses. The implication from

(18) Piraino, P.; Bruno, G.; Lo Schiavo, S.; Laschi, F.; Zanello, P. *Inorg. Chem.* **1987**, *26*, 2205.

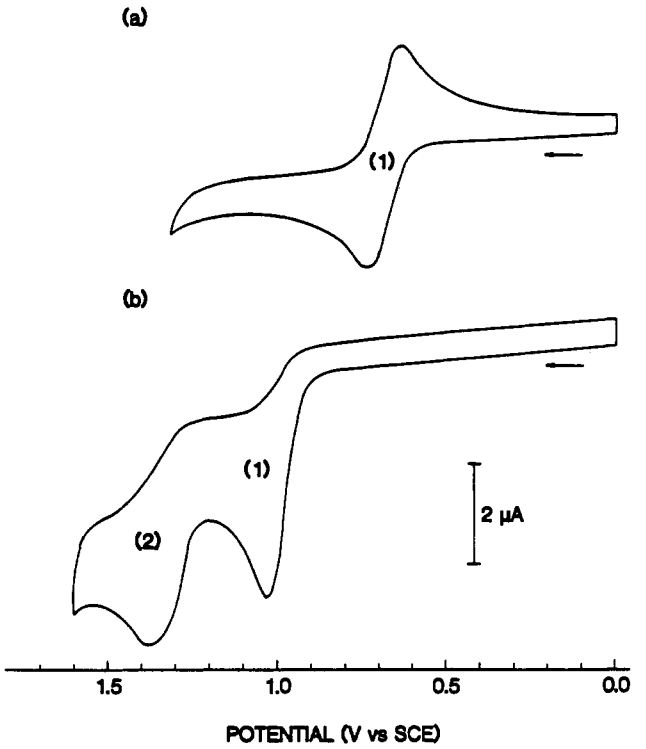

Figure 3. Cyclic voltammograms of (a) 1.8×10^{-3} M $Pd_2(\mu\text{-dpb})_4$ and (b) 2.5×10^{-3} M $[(dpb)Pd]_2(\mu\text{-dpb})_2$ in CH_2Cl_2, 0.1 M TBAP (scan rate 0.1 V/s).

the present study is that other such intermediate complexes may exist en route to analogous binuclear complexes M_2L_4 with M = Rh, Pd, Ni, etc., but they may not be so stable as the dpb complex. We have tried the same preparation method with 2-anilinopyridine, but X-ray structure analysis of the product showed that the tetrabridged complex is formed directly with no chelate intermediate being detected.[19] Why the dpb imparts such stability to the chelated complex is still unanswered at this time.

Electrochemical and Spectroscopic Studies. Figure 3 shows the cyclic voltammograms of **1** and **2** in CH_2Cl_2, 0.1 M TBAP at a platinum electrode. No reduction wave was observed for either complex up to −1.8 V in this solvent. Compound **1** shows two irreversible oxidation waves, in that no corresponding cathodic waves are observed (Figure 3b). The anodic peak potentials at 100 mV/s for these waves are at $E_p(1) = 1.02$ V and $E_p(2) = 1.26$ V. However, the wave analysis for the first oxidation shows a constant $i_p/v^{1/2}$ ratio and $E_p - E_{p/2} = 60 \pm 10$ mV, indicating a diffusion-controlled electron-transfer process. The second wave is much broader, and the peak potential shifts in the anodic direction as the scan rate is increased. The above behavior for the two waves is characteristic of an ECE mechanism where the first oxidation involves a reversible electron transfer followed by a chemical reaction to give a product that is subsequently irreversibly oxidized to give the second wave. The room-temperature and low-temperature cyclic voltammograms of **1** at various scan rates are shown in Figure 4. At 24 °C, they do not show any corresponding cathodic wave as the scan rate varies from 0.1 to 0.4 V/s (Figure 4a), whereas at −78 °C, the cathodic wave clearly is visible (Figure 4b). The observed cathodic wave is due to the reduction of the oxidized form of compound **1**, which has an increased lifetime at −78 °C. The ratio of the cathodic peak current vs anodic peak current (i_{pc}/i_{pa}) varies from 0.36 at 0.1 V/s to 0.71 at 0.4 V/s, indicating the effect of the scan rate on the peak current ratio at this temperature. This ratio is directly related to the rate of the chemical reaction following electrooxidation of **1**.

Bulk controlled-potential electrolysis of **1** at +1.15 V reveals that a total of 1.9 ± 0.1 electrons is involved in the first oxidation.

(19) Bear, J. L.; He, L.-P.; Yao, C.-L., unpublished results.

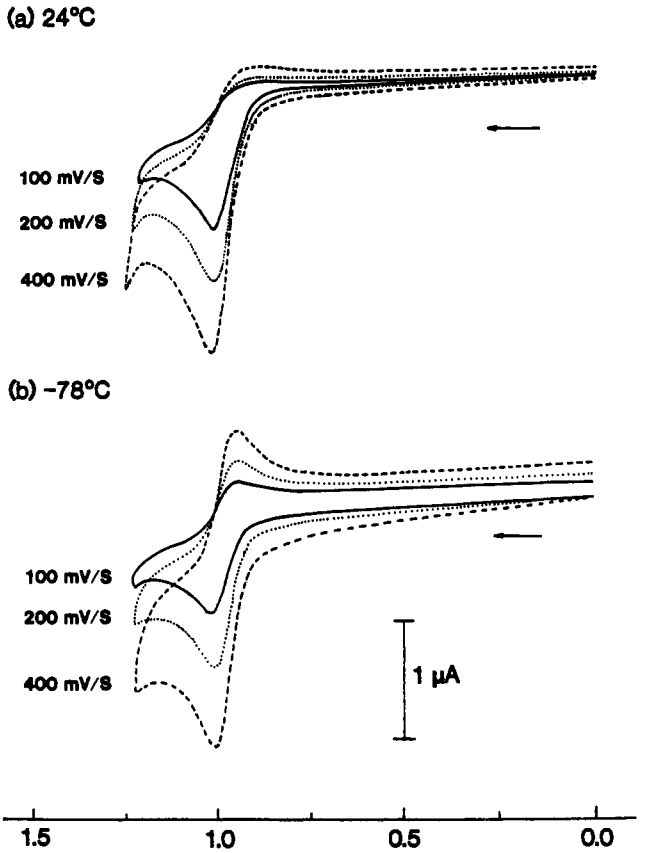

Figure 4. Cyclic voltammograms of 1.5×10^{-3} M $[(dpb)Pd]_2(\mu\text{-dpb})_2$ in CH_2Cl_2, 0.1 M TBAP with various scan rates at (a) 24 °C and (b) −78 °C.

Figure 5. ESR spectrum of singly oxidized $Pd_2(\mu\text{-dpb})_4$ at 123 K in CH_2Cl_2, 0.1 M TBAP.

These data, together with the results obtained from cyclic voltammetry, indicate a two-electron-transfer process with two noninteracting palladium(II) ions.[20] No ESR signal was observed for the oxidation product. Also an attempt to rereduce the bulk oxidized complex at 0.0 V resulted in no current flow at the electrode, indicating the oxidized species undergoes a rapid chemical reaction. These results further support an ECE electrochemical mechanism. The nature of the chemical reaction after oxidation is not known at this time.

The cyclic voltammogram for compound **2** shown in Figure 3a displays a reversible one-electron oxidation at $E_{1/2} = 0.65$ V vs SCE in CH_2Cl_2, 0.1 M TBAP. A one-electron process is confirmed by bulk controlled-potential electrolysis of **2** at +0.70 V, which shows that a total of 0.9 ± 0.1 electrons is involved in the reversible oxidation. No other reversible oxidation was observed up to the limit of the solvent (+1.6 V). This result is different from that reported for $Pd^{II}_2(dtf)_4$, where two reversible one-electron

(20) Flanagan, J. B.; Margel, S. J.; Bard, A. J.; Anson, F. C. *J. Am. Chem. Soc.* **1978**, *100*, 4248.

Table IV. Atomic Coordinates ($\times 10^4$) and Equivalent Isotropic Displacement Parameters (Å $\times 10^3$)

	$[(dpb)Pd]_2(\mu\text{-dpb})_2$				$Pd_2(\mu\text{-dpb})_4$			
atom	*x*	*y*	*z*	*U*(eq)[a]	*x*	*y*	*z*	*U*(eq)[a]
Pd(1)	7244 (1)	5601 (1)	1165 (1)	41 (1)	2374 (1)	1152 (1)	1902 (1)	32 (1)
Pd(2)	7536 (1)	4379 (1)	1151 (1)	44 (1)	1563 (1)	905 (1)	1182 (1)	34 (1)
N(1)	7897 (5)	4779 (6)	775 (6)	39 (8)	1838 (4)	758 (4)	2463 (4)	34 (4)
N(2)	7453 (5)	5675 (6)	530 (6)	36 (7)	1246 (4)	369 (3)	1776 (4)	33 (4)
N(3)	6916 (5)	4429 (7)	314 (6)	40 (8)	2757 (4)	420 (4)	1691 (4)	35 (4)
N(4)	6592 (5)	5272 (7)	485 (7)	48 (9)	2147 (5)	324 (5)	911 (4)	36 (4)
N(5)	7294 (5)	3906 (7)	1631 (7)	56 (10)	2817 (4)	1530 (4)	1266 (4)	35 (4)
N(6)	8067 (6)	4083 (8)	2045 (7)	70 (11)	1989 (5)	1466 (4)	680 (4)	37 (4)
N(7)	7193 (5)	5708 (7)	1958 (6)	58 (9)	1886 (5)	1853 (4)	2017 (4)	37 (4)
N(8)	7827 (5)	5944 (7)	1923 (7)	53 (9)	1069 (4)	1518 (4)	1531 (4)	39 (5)
C(1)	7763 (7)	5309 (10)	496 (8)	41 (5)	1423 (6)	413 (5)	2298 (6)	34 (4)
C(2)	8315 (6)	4471 (9)	865 (7)	43 (5)	1857 (4)	960 (3)	3016 (3)	32 (4)
C(3)	8287 (6)	3867 (8)	768 (7)	44 (5)	2399	961	3307	48 (4)
C(4)	8697 (7)	3530 (9)	896 (8)	65 (6)	2431	1202	3830	53 (4)
C(5)	9132 (7)	3826 (9)	1122 (9)	68 (6)	1919	1441	4063	75 (5)
C(6)	9170 (7)	4419 (10)	1215 (8)	68 (6)	1378	1439	3772	85 (5)
C(7)	8754 (6)	4755 (9)	1102 (8)	56 (6)	1346	1199	3249	59 (5)
C(8)	7990 (6)	5523 (8)	118 (7)	42 (5)	1124 (4)	56 (3)	2723 (3)	38 (4)
C(9)	7959 (6)	5171 (8)	−370 (8)	54 (6)	500	48	2779	56 (5)
C(10)	8183 (7)	5392 (9)	−699 (9)	70 (6)	233	−288	3176	77 (5)
C(11)	8399 (7)	5938 (10)	−539 (10)	77 (7)	589	−616	3515	84 (6)
C(12)	8447 (7)	6270 (9)	−61 (9)	67 (6)	1214	−608	3458	68 (5)
C(13)	8228 (6)	6069 (8)	265 (8)	53 (6)	1481	−272	3062	47 (4)
C(14)	7230 (6)	6139 (8)	103 (8)	32 (5)	947 (4)	−113 (3)	1578 (3)	37 (4)
C(15)	6966 (6)	6045 (9)	−540 (8)	53 (6)	417	−60	1273	44 (4)
C(16)	6720 (7)	6523 (10)	−958 (10)	75 (7)	147	−521	1042	65 (5)
C(17)	6748 (8)	7089 (11)	−705 (10)	83 (7)	407	−1035	1115	70 (5)
C(18)	7024 (7)	7183 (10)	−69 (10)	71 (7)	937	−1088	1420	63 (5)
C(19)	7264 (6)	6717 (8)	338 (8)	49 (5)	1207	−627	1651	48 (4)
C(20)	6550 (7)	4786 (10)	148 (8)	43 (5)	2610 (6)	165 (5)	1223 (6)	37 (4)
C(21)	6896 (6)	4001 (9)	−118 (9)	46 (5)	3110 (3)	140 (3)	2096 (3)	31 (4)
C(22)	6963 (7)	3395 (10)	54 (10)	73 (7)	2971	−393	2255	50 (4)
C(23)	6964 (8)	2960 (11)	−354 (10)	86 (7)	3323	−658	2651	66 (5)
C(24)	6897 (8)	3121 (11)	−909 (11)	94 (8)	3814	−391	2888	58 (5)
C(25)	6831 (8)	3718 (11)	−1095 (11)	93 (8)	3952	143	2729	59 (5)
C(26)	6837 (6)	4152 (9)	−681 (9)	60 (6)	3601	408	2333	44 (4)
C(27)	6073 (7)	4672 (9)	−445 (8)	50 (5)	2975 (4)	−307 (3)	1023 (3)	37 (4)
C(28)	5881 (7)	5069 (10)	−929 (9)	66 (6)	2699	−795	866	51 (4)
C(29)	5434 (8)	4916 (11)	−1508 (11)	92 (8)	3048	−1232	680	67 (5)
C(30)	5220 (8)	4400 (11)	−1557 (10)	87 (7)	3672	−1181	652	84 (5)
C(31)	5394 (8)	4012 (10)	−1098 (10)	79 (7)	3948	−694	810	82 (6)
C(32)	5826 (7)	4148 (9)	−531 (9)	63 (6)	3599	−257	995	53 (5)
C(33)	6189 (7)	5592 (9)	390 (7)	49 (5)	2081 (4)	173 (3)	341 (3)	36 (4)
C(34)	5804 (7)	5317 (9)	408 (8)	63 (6)	1523	−18	161	53 (4)
C(35)	5415 (8)	5687 (11)	351 (9)	85 (7)	1426	−119	−400	66 (5)
C(36)	5422 (8)	6275 (11)	286 (9)	78 (7)	1887	−30	−782	76 (5)
C(37)	5797 (8)	6560 (11)	288 (9)	87 (7)	2445	160	−602	71 (5)
C(38)	6165 (7)	6217 (9)	330 (8)	64 (6)	2542	262	−40	60 (4)
C(39)	7733 (9)	3785 (9)	2108 (10)	57 (6)	2527	1635 (5)	798 (6)	34 (4)
C(40)	6862 (7)	3623 (9)	1467 (8)	52 (6)	3444 (3)	1587 (4)	1315 (4)	49 (4)
C(41)	6813 (8)	3013 (10)	1437 (9)	76 (7)	3847	1295	987	82 (5)
C(42)	6371 (9)	2750 (12)	1276 (10)	99 (8)	4465	1361	1062	95 (6)
C(43)	5971 (9)	3098 (11)	1138 (10)	98 (8)	4679	1720	1465	86 (6)
C(44)	6012 (9)	3733 (12)	1164 (10)	101 (8)	4276	2013	1793	96 (6)
C(45)	6477 (7)	3992 (10)	1338 (9)	69 (6)	3658	1946	1718	76 (5)
C(46)	7841 (7)	3353 (9)	2628 (9)	59 (6)	2851 (3)	1975 (4)	361 (4)	59 (5)
C(47)	7568 (7)	3392 (9)	2924 (9)	64 (6)	2951	1754	−163	89 (6)
C(48)	7672 (8)	2945 (10)	3382 (10)	81 (7)	3274	2049	−558	123 (7)
C(49)	8004 (8)	2503 (11)	3519 (11)	92 (8)	3497	2566	−428	126 (7)
C(50)	8260 (9)	2483 (12)	3236 (11)	108 (9)	3396	2788	96	105 (6)
C(51)	8184 (7)	2922 (9)	2780 (9)	74 (7)	3073	2492	490	69 (5)
C(52)	8529 (8)	4181 (8)	2532 (9)	55 (6)	1652 (3)	1709 (4)	244 (3)	49 (4)
C(53)	8633 (8)	4372 (10)	3101 (10)	82 (7)	1477	1392	−209	60 (5)
C(54)	9103 (8)	4508 (10)	3599 (11)	94 (8)	1094	1610	−609	102 (6)
C(55)	9481 (9)	4426 (11)	3498 (11)	98 (8)	884	2145	−557	95 (6)
C(56)	9383 (8)	4201 (9)	2931 (10)	85 (7)	1058	2462	−104	76 (5)
C(57)	8920 (8)	4091 (9)	2448 (10)	76 (7)	1442	2244	296	67 (5)
C(58)	7639 (8)	5899 (9)	2291 (9)	52 (6)	1330 (7)	1892 (5)	1856 (6)	35 (4)
C(59)	6933 (7)	5447 (8)	2212 (8)	50 (5)	2206 (3)	2320 (3)	2201 (4)	42 (4)
C(60)	7146 (8)	5042 (10)	2683 (9)	69 (6)	2268	2778	1861	47 (4)
C(61)	6885 (9)	4768 (10)	2937 (11)	90 (8)	2636	3210	2025	62 (5)
C(62)	6395 (9)	4946 (11)	2672 (10)	94 (8)	2943	3184	2529	82 (5)
C(63)	6188 (9)	5352 (10)	2200 (10)	88 (7)	2881	2726	2868	101 (6)
C(64)	6452 (7)	5614 (10)	1960 (9)	76 (6)	2512	2294	2704	71 (5)
C(65)	7919 (7)	6043 (8)	2981 (8)	51 (6)	958 (3)	2387 (3)	2027 (4)	40 (4)

Table IV (Continued)

	$[(dpb)Pd]_2(\mu\text{-dpb})_2$				$Pd_2(\mu\text{-dpb})_4$			
atom	*x*	*y*	*z*	*U*(eq)[a]	*x*	*y*	*z*	*U*(eq)[a]
C(66)	8386 (7)	5868 (8)	3342 (8)	56 (6)	938	2544	2582	59 (4)
C(67)	8406 (8)	6263 (10)	4240 (11)	88 (7)	590	2992	2742	68 (5)
C(68)	8640 (8)	5975 (10)	3996 (10)	89 (7)	263	3282	2346	74 (5)
C(69)	7962 (8)	6443 (10)	3915 (10)	78 (7)	284	3126	1791	76 (5)
C(70)	7694 (8)	6335 (9)	3245 (10)	73 (6)	631	2678	1631	62 (5)
C(71)	8241 (7)	6251 (9)	2066 (8)	53 (6)	441 (3)	1472 (3)	1461 (4)	35 (4)
C(72)	8574 (8)	5944 (11)	1989 (9)	86 (7)	48	1490	1911	58 (4)
C(73)	9021 (10)	6246 (14)	2112 (12)	126 (10)	−569	1430	1827	76 (5)
C(74)	9080 (10)	6811 (13)	2280 (11)	116 (9)	−794	1353	1294	78 (5)
C(75)	8769 (9)	7125 (13)	2356 (11)	109 (9)	−401	1336	843	72 (5)
C(76)	8333 (8)	6833 (10)	2247 (9)	76 (7)	216	1396	927	56 (5)
O(77)[b]	10387 (9)	8670 (12)	2073 (12)	105 (9)	9472 (33)	4552 (29)	128 (31)	120
O(78)[b]	10798 (14)	2018 (19)	2282 (18)	108 (14)	8924 (35)	4860 (32)	302 (30)	120
O(80)[b]	4676 (14)	2727 (19)	1379 (18)	101 (13)	9281 (21)	5362 (20)	478 (19)	120
C(81)	4722 (25)	3285 (36)	1486 (33)	135 (25)				
O(82)	4751 (24)	7729 (31)	496 (30)	148 (24)				
C(83)	5006 (34)	8075 (43)	251 (41)	129 (33)				
O(84)	4814 (24)	7438 (29)	2551 (33)	115 (26)				
C(85)	4365 (28)	7327 (34)	2418 (33)	114 (23)				
O(86)	5188 (19)	9034 (25)	−1268 (25)	117 (19)				
C(87)	5029 (31)	8898 (40)	−688 (40)	120 (31)				

[a] Equivalent isotropic *U* defined as one-third of the trace of the orthogonalized U_{ij} tensor. [b] The last three atoms for compound **2** are C(77), C(78), and O, respectively.

oxidations were reported at +0.81 and +1.19 V vs Ag/AgCl in CH_2Cl_2, 0.1 M $TBAPF_6$.[11] The difference between the first and second oxidation potentials for $Pd^{II}_2(dtf)_4$ is 0.38 V. If the same potential difference is used for the $Pd_2(\mu\text{-dpb})_4$ complex, the second oxidation potential should occur near 1.03 V, which is not observed.

Figure 5 shows the ESR spectrum of a frozen solution (123 K) of the product formed after bulk electrolysis of $Pd^{II}_2(\mu\text{-dpb})_4$ in CH_2Cl_2 at +0.70 V. The ESR spectrum clearly shows an axial signal with $g_\perp = 2.17$ and $g_\parallel = 1.98$. The satellite peaks ($A_\perp = 33 \times 10^{-4}$ cm^{-1} and $A_\parallel = 39 \times 10^{-4}$ cm^{-1}) are due to the ^{105}Pd ($I = {}^5/_2$, natural abundance 22.3%). The ESR results show that the oxidation is metal centered and that a $Pd^{II}Pd^{III}$ complex is formed. The ESR spectrum of $[Pd^{II}Pd^{III}(\mu\text{-dpb})_4]^+$ is similar to that reported for the isoelectronic complex $[Rh^{I}Rh^{II}(\mu\text{-dpb})_4]^-$.[3] The latter complex gives an axial signal with $g_\perp = 2.181$ and $g_\parallel = 2.003$. Both signals are split into 1/2/1 triplets with $A_\perp = 9 \times 10^{-4}$ cm^{-1} and $A_\parallel = 16 \times 10^{-4}$ cm^{-1}, showing that the odd electron is equally distributed over both rhodium ions (nuclear spin of ${}^1/_2$ for each ^{103}Rh). It is not possible to determine the spin distribution of the odd electron in $[Pd^{II}Pd^{III}(\mu\text{-dpb})_4]^+$ since the concentration of the complex with the isotope combination ^{105}Pd–^{105}Pd would be very low. However, the odd-electron orbital should be M–M σ^*, as is the case for $[Rh^{I}Rh^{II}(\mu\text{-dpb})_4]^-$.

The oxidation potentials of **1** and **2** show the effect of the proximity of the two palladium ions on the HOMO energies of the two molecules. For **1** the two noninteracting palladium ions are both oxidized at 1.02 V. When the two palladium ions are forced into close contact by the four bridging ligands (compound **2**), the metal-centered HOMO is raised in energy by 370 mV. Under these conditions, the oxidation of **2** involves only one electron per dimer forming the radical cation. The loss of one electron results in an increase in positive charge on the complex and a Pd–Pd bonding interaction. These factors combine to lower the energy of the HOMO, and a second reversible metal-centered oxidation is not observed. An irreversible oxidation process is observed at a potential greater than 1.6 V that overlaps with the solvent discharge wave. If this irreversible wave corresponds to the formation of a Pd^{III}_2 compound, it is not stable under the conditions of the experiment and undergoes decomposition.

In summary, the reaction of Li(dpb) with the palladium acetate trimer in CH_2Cl_2 results in the formation of compound **1**. This is the first example of this type of reaction intermediate ever reported. It is not clear whether the formation of a dibridged complex is unique for this chemical system or if a structurally similar intermediate is common in the syntheses of other tetrabridged dipalladium compounds. Compound **1** is quite reactive and can be converted into compound **2** by refluxing in a methanol solution. The difference in the electrochemistry of **1** and **2** is a result of the Pd···Pd interaction in the Pd^{II}_2 and $Pd^{II}Pd^{III}$ tetrabridged complexes. Apparently the higher energy HOMO in **2** results from the forced proximity of the two square-planar d^8 palladium centers. The strongest repulsion should occur between the two filled d_{z^2} orbitals, which upon the loss of one electron gives a bonding state with the odd electron in a Pd–Pd σ^* orbital. The ESR spectrum of the radical cation, $Pd^{II}Pd^{III}$, shows axial symmetry with the six satellite peaks expected for ^{105}Pd (22.3% abundance). These results are consistent with the odd-electron orbital being metal centered and possessing axial symmetry. The electrochemical properties of **2** and the ESR spectrum of $[Pd^{II}Pd^{III}(dpb)_4]^+$ are quite different from those reported for $Pd^{II}_2(dtf)_4$ and $[Pd^{II}Pd^{III}(dtf)_4]^+$. This was unexpected, since the electrochemistry and ESR spectra of the corresponding dpb, dpf, and dtf complexes of dirhodium(II) and -(II,III) are similar.

Acknowledgment. The support of the Robert A. Welch Foundation (Grant No. E-918) is gratefully acknowledged.

Registry No. **1**, 117144-68-0; **1**(H_2O)(MeOH), 117144-69-1; **2**, 117120-37-3; **2**(EtOH), 117120-38-4; $\mathbf{2}^+$, 117120-39-5.

Supplementary Material Available: For **1** and **2**, Tables S1–S3, listing data collection processing parameters, hydrogen atomic coordinates and isotropic thermal parameters, and anisotropic thermal parameters, and Figures S1 and S2, showing packing diagrams (6 pages); Tables S4 and S5, listing observed and calculated structure factors for **1** and **2** (22 pages). Ordering information is given on any current masthead page.